Journal of Power Sources 189 (2009) 1251–1255

Contents lists available at ScienceDirect

Journal of Power Sources

journal homepage: www.elsevier.com/locate/jpowsour

Short communication

Improved electrochemical properties of amorphous $Mg_{65}Ni_{27}La_8$ electrodes: Surface modification using graphite

D.C. Wu, Lu Li, G.Y. Liang*, Y.L. Guo, H.B. Wu

Department of Material Physics, School of Science, Xi'an Jiaotong University, Xi'an 710049, China

ARTICLE INFO

Article history:
Received 21 October 2008
Received in revised form
26 November 2008
Accepted 26 November 2008
Available online 25 December 2008

Keywords:
Amorphous alloy
Surface modification
Electrochemical properties
Ni–MH batteries

ABSTRACT

Amorphous $Mg_{65}Ni_{27}La_8$ alloy is prepared by melt-spinning. The alloy surface is modified using different contents of graphite to improve the performances of the $Mg_{65}Ni_{27}La_8$ electrodes. In detail, the electrochemical properties of $(Mg_{65}Ni_{27}La_8)+xC$ ($x=0$–0.4) electrodes are studied systematically, where x is the mass ratio of graphite to alloy. Experimental results reveal that the discharge capacity, cycle life, discharge potential characteristics and electrochemical kinetics of the electrodes are all improved. The surface modification enhances the electrocatalytic activity of the alloy, reduces the contact resistance of the electrodes and obstructs the formation of $Mg(OH)_2$ on the alloy surface. An optimal content of graphite has been obtained. The $(Mg_{65}Ni_{27}La_8)+0.25$ C electrode has the largest discharge capacity of 827 mA h g^{-1}, which is 1.47 times as large as that of the electrode without graphite, and the best electrochemical kinetics. Further increasing of graphite content will lead to the increase of contact resistance and activation energy for charge-transfer reaction of the electrode, resulting in the degradation of electrode performance.

1. Introduction

Mg-based hydrogen-storage alloys are considered as one of the most promising candidates for the 3rd generation negative materials of Ni–MH batteries, because of their high discharge capacity and rich natural resources [1]. However, the practical application of Mg-based alloys is restrained by their poor hydriding–dehydriding kinetics at room temperature and their poor charge/discharge cycle stability caused by the formation of $Mg(OH)_2$ on the surface of alloys in alkaline solution. In order to overcome such disadvantages, many methods have been adopted. One of them is preparation non-equilibrium structured alloys by ball milling [2,3] or rapid solidification [4,5]. These alloys usually exhibit higher discharge capacities at room temperature [6–9]. Another of them is the surface modification [10].

A few studies about influence of carbon on the characteristics of Mg-based alloys have been reported. Iwakura et al. [11–13] reported that both the discharge capacity and the charge/discharge cycle life of MgNi electrode are improved by surface modification with 20 wt.% graphite. They proposed that the surface modification leads to an increase of Ni/Mg ratio on the surface of alloy. They also found that there is an optimal time for the modification by planetary milling, which is 10 min. In contrast, Ruggeri et al. [14] found that surface modification of MgNi by ball milling the mixture of alloy and graphite for 10 h has a major deleterious effect on the discharge capacity, because carbon limits the charge-transfer reaction at the surface of the alloy. In addition, Funaki et al. [15] prepared $MgNiC_x$ up to $x=1.31$ by mechanical alloying of amorphous MgNi and graphite for 20 h, and found that that carbon atoms dissolved into the sites that otherwise would be occupied by hydrogen atoms. Guo et al. [16] studied the effect of surface modification of amorphous $MgNi_{1+x}$ ($x=0.05$–0.3) by introduction of various carbon sources in the system (graphite, CNTs and carbon black), and found that graphite could increase the surface electrocatalytic activity and the cycle life of the electrodes effectively. According to the above results, graphite is a reasonable material for surface modification, and the milling time for modification should not be long. Otherwise, graphite could block the hydrogen interstitial sites, resulting in the decreasing of the discharge capacity of the electrodes. To the best of our knowledge, a systematic study of the influence of different graphite contents for modification on the electrode characteristics is needed.

The amorphous alloy prepared by melt-spinning has a better cycling stability than that prepared by mechanical alloying [17]. Thus, on the present work, melt-spinning technique is employed to prepare the amorphous $Mg_{65}Ni_{27}La_8$ alloy. The rare earth element La is added to enhance the glass forming ability of the alloy. The aim of this paper is to investigate the electrode characteristics of amorphous $Mg_{65}Ni_{27}La_8$ by surface modification using graphite. A systematic comparison on the effects of surface modification using different contents of graphite is carried out. The effects of surface modification are discussed on the basis of the morphology, limiting current density, activation energy for charge-transfer

* Corresponding author. Tel.: +86 29 82663747; fax: +86 29 83207910.
E-mail addresses: dcwu@2008.sina.com (D.C. Wu), gyliang@mail.xjtu.edu.cn (G.Y. Liang).

0378-7753/$ – see front matter.
doi:10.1016/j.jpowsour.2008.11.145

reaction and electrochemical impedance spectra of the electrodes.

2. Experimental

$Mg_{65}Ni_{27}La_8$ alloy ingots were prepared by melting a mixture of La (99.8 wt.%) metal and Mg–Ni intermediate alloy (99.6 wt.%) in a vacuum induction furnace under the protection of argon gas. The detailed preparation procedures have been given elsewhere [5]. The amorphous ribbons were produced by a single roller melt-spun technique (copper quenching disc with a diameter of 250 mm and surface velocity of about 39 m s^{-1}) in an argon atmosphere of 400 mbar. The as-quenched ribbons were then ball-milled into powder using a SPEX 8000 Mixer Mill for 7 min, with a ball-to-powder mass ratio of 30:1. The stainless steel jar was sealed with a rubber O ring under argon atmosphere in a glove box before operation. Then, the $Mg_{65}Ni_{27}La_8$ powder was mixed with Ni powder and graphite powder (300 mesh) with a mass ratio of 1:4:x (x = 0, 0.15, 0.25, 0.4) in a mortar. These mixtures were milled for another 3 min in the same condition for the surface modifications of $Mg_{65}Ni_{27}La_8$ powder. The $Mg_{65}Ni_{27}La_8$ alloy could retain the amorphous structure after 10 min of milling [18], and the graphite only stayed at the surface of the alloy [16]. The test negative electrodes were fabricated by cold pressing the resultant powders into pieces of nickel foam under a pressure of 20 MPa. The electrodes were represented as $(Mg_{65}Ni_{27}La_8)+xC$ (x = 0, 0.15, 0.25, 0.4) base on the different graphite content.

Electrochemical measurements were made at room temperature (27 ± 1 °C) in 6 M KOH solution containing 20 g L^{-1} LiOH using a three-electrode cell. The positive and reference electrode were NiOOH/$Ni(OH)_2$ and Hg/HgO, respectively. Charge/discharge cycles were carried out with an Arbin BT2000 battery tester. The electrode was charged at 100 mA g^{-1} for 10 h and discharged at 50 mA g^{-1}, and the cut-off potential was set to −0.5 V (vs. Hg/HgO).

Scanning electron microscopy (SEM) observations of the morphology of the powders were carried out using a Jeol JSM-7000F microscope equipped with energy dispersive X-ray detector (EDX).

After the electrodes were completely activated by cycling, the anode polarization, the linear polarization and the electrochemical impedance spectroscopy (EIS) studies were conducted at 50% depth of discharge (DOD) using AMETEK VersaSTAT MC electrochemical test system. The anode polarization and the EIS test were carried out at room temperature (27 ± 1 °C), and the linear polarization was performed in a temperature-controlled bath in the range of 0–40 °C. The anode polarization and the linear polarization curves were measured by scanning the electrode potential at a rate of 5 mV s^{-1} from 0 to 600 mV (versus open circuit potential) and 0.1 mV s^{-1} from −5 to 5 mV (versus open circuit potential), respectively. The EIS of the electrodes were obtained in the frequency range of 10 kHz to 5 mHz with an AC amplitude of 5 mV under the open circuit condition. The software of the test system was used to analyze the data of EIS.

3. Results and discussion

Fig. 1 shows discharge capacities as a function of cycle number for the $(Mg_{65}Ni_{27}La_8)+xC$ (x = 0–0.4) negative electrodes. The discharge capacity is greatly improved by surface modification using graphite. The maximum discharge capacity of each electrode increases first and then decreases with increasing graphite content. The $(Mg_{65}Ni_{27}La_8)+0.25$ C negative electrode has the largest discharge capacity of 827 mA h g^{-1}, which is 1.47 times as large as that of graphite-free electrode, as shown in Table 1. Obviously, there is an optimal graphite content for the preparation of the amorphous $Mg_{65}Ni_{27}La_8$ electrode with high discharge capacity. Table 1 also gives the cycle numbers needed to activate each electrode and the capacity retention of each electrode after 20 cycles. The graphite can slightly expedite the process of activation and improve the capacity retention after 20 cycles, indicating the improvement of charge/discharge cycle life.

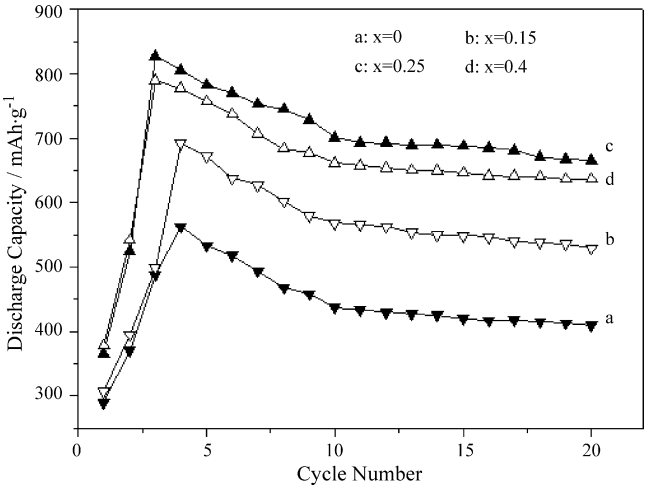

Fig. 1. Discharge capacities as a function of cycle number for the $(Mg_{65}Ni_{27}La_8)+xC$ (x = 0–0.4) negative electrodes. The charge and discharge current densities are 100 mA h g^{-1} and 50 mA h g^{-1}, respectively.

Increase of the discharge capacity and better activation property are believed to be caused by an increasing of active sites for hydrogen absorption and desorption on the surface of amorphous $Mg_{65}Ni_{27}La_8$ alloy, which might involving some chemical state modification of Mg and Ni on the alloy surface [11]. Aymard et al. [19] reported that a fracture of the graphite layers occurred during milling, which generated small particles with free dangling bonds. We think these graphite particles with free dangling bonds will react with Mg and Ni atoms on the alloy surface, which causes chemical state modification on the surface of alloy.

Fig. 2 is a SEM image of a Ni particle of the $Mg_{65}Ni_{27}La_8$ electrode. The Ni particle has a large surface area. Many $Mg_{65}Ni_{27}La_8$ particles are embeded in the Ni particle after milling, because there are many protuberances on the surface of Ni particle. There are some imaginable gaps between Ni and $Mg_{65}Ni_{27}La_8$ particles, so the electric conductivity of the electrode will be lower. However, for the electrodes containing graphite, these gaps will be partially filled with graphite particles. Because graphite is conductive, the contact resistance between them will be reduced. This is helpful to improve the discharge capacity and activation property.

Usually, the decreasing of discharge capacity is attributed to the formation of $Mg(OH)_2$ on the surface of alloy during the charge/discharge cycles in alkaline solution. The formation of $Mg(OH)_2$ leads to a loss of hydrogen-storage materials and obstructs the diffusion of hydrogen atoms [20]. The initial activation of the electrodes could be ascribed to the cracking of alloy particles during charge/discharge cycles, which generates fissures on the surface of alloy. These fissures will speed up the corrosion of the electrode. Fig. 3(a) shows the surface of $Mg_{65}Ni_{27}La_8$ particle of the $(Mg_{65}Ni_{27}La_8)+0.15$ C electrode after 10 cycles. Fissures are

Table 1
Electrochemical properties of the $(Mg_{65}Ni_{27}La_8)+xC$ (x = 0–0.4) alloy electrodes.

Samples	C_{max} (mA h g^{-1})	N_a [a]	C_{20}/C_{max} [b] (%)
x = 0	558.0	4	72.8
x = 0.15	691.9	4	76.5
x = 0.25	827.1	3	80.4
x = 0.4	789.2	3	80.7

[a] The cycle numbers needed to activate the electrodes.
[b] The capacity retention of samples at the 20th cycle.

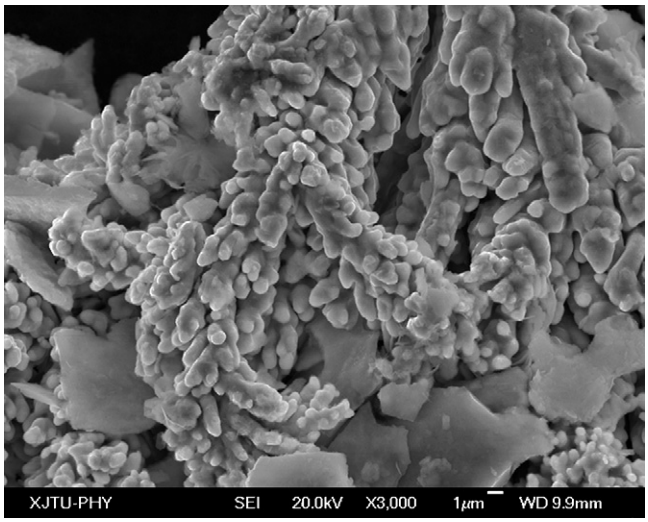

Fig. 2. SEM image of a Ni particle of the $Mg_{65}Ni_{27}La_8$ electrode.

also formed on the alloy surface, and most of the areas are covered with bacilliform $Mg(OH)_2$. However, in some area (marked using red circle), little $Mg(OH)_2$ is observed. These areas are covered with graphite, indicating the surface modification by graphite can obstruct the formation of $Mg(OH)_2$. Besides, it seems that at least two pieces of graphite are embed in a fissure (marked using arrow in Fig. 3(a)). The results of EDX line scan (see Fig. 3(b)) confirms that they are graphite. The graphite on the alloy surface and in the fissure is beneficial to slowdown the corrosion and to improve the cycle life of the electrode. The results of EDX line scan also show that the concentration of carbon on the corroded area is less than 10%. It suggests that when the concentration of graphite is small, its effect on preventing the corrosion is weak.

The discharge potential characteristics are characterized by the potential plateau of the discharge potential curve of the electrodes. The longer and the more horizontal the potential plateau is, the better the potential characteristics of the electrodes are. Fig. 4 presents discharge potential curves of the $(Mg_{65}Ni_{27}La_8)+xC$ ($x=0$–0.4) electrodes at the 10th cycle. The potential plateau becomes more horizontal with increasing graphite content. The surface modification also decreases the discharge potential and increases the length

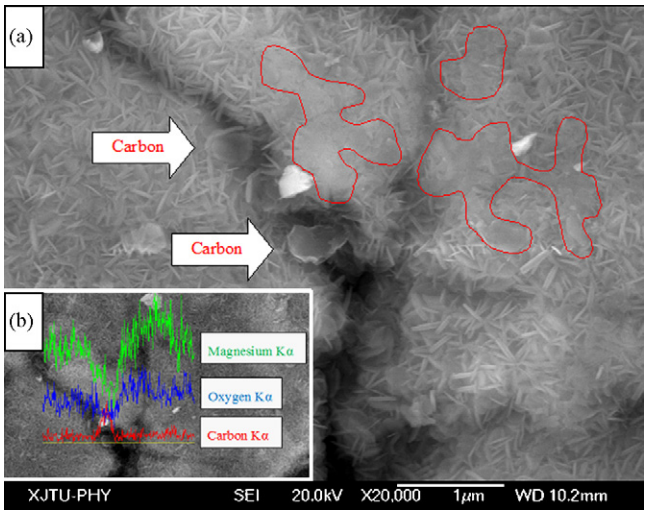

Fig. 3. SEM image of the surface of $Mg_{65}Ni_{27}La_8$ particle ($(Mg_{65}Ni_{27}La_8)+0.15$ C electrode) after 10 cycles (a), together with the EDX line scan of Mg Kα, O Kα and C Kα (b).

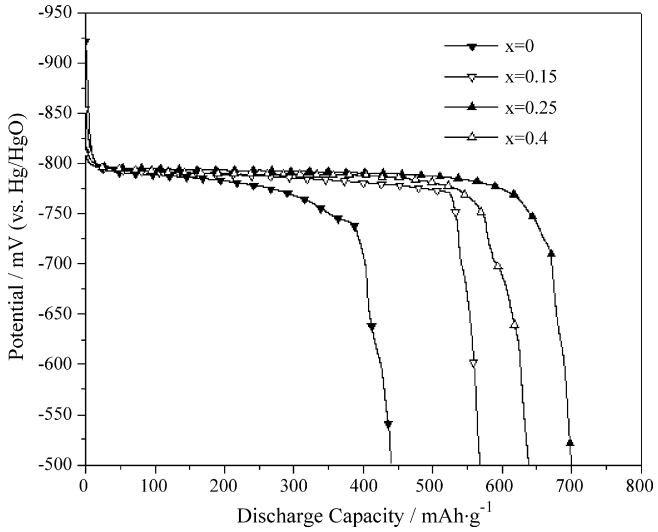

Fig. 4. Discharge potential curves of the $(Mg_{65}Ni_{27}La_8)+xC$ ($x=0$–0.4) electrodes at the 10th cycle.

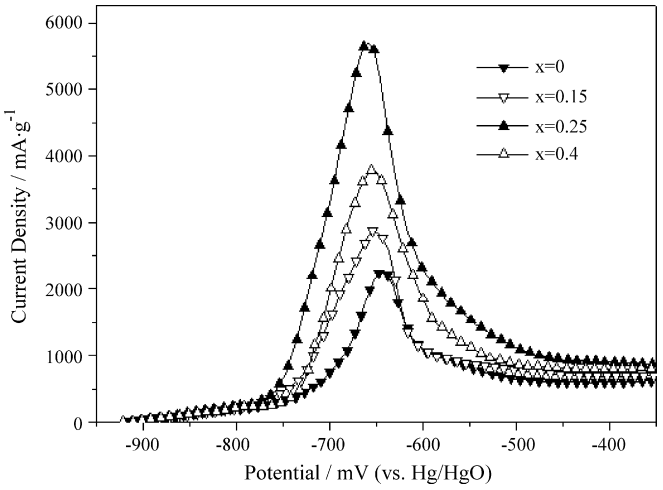

Fig. 5. Anode polarization curves of the $(Mg_{65}Ni_{27}La_8)+xC$ ($x=0$–0.4) electrodes at 50% depth of discharge at 27 °C.

of potential plateau compared to the graphite-free electrode, suggesting the decrease of hydrogen overpotential or the increase of the electrocatalytic activity.

Fig. 5 shows anode polarization curves of the $(Mg_{65}Ni_{27}La_8)+xC$ ($x=0$–0.4) electrodes. In all cases, the anodic current densities increase to a limiting value and then decrease. The anodic peaks correspond to the oxidation of hydrogen, because they are measured at 50% DOD. The limiting current density I_L is listed in Table 2. It increases first from 2263.4 mA g^{-1} ($x=0$) to 5692.3 mA g^{-1} ($x=0.25$) and then decreases to 3775.6 mA g^{-1} ($x=0.4$), which implies the electrochemical kinetics of the electrodes increases first and then decreases with increasing graphite content.

Table 2
Limiting current density I_L (27 °C) and activation energy E_a for the charge-transfer reaction of the $(Mg_{65}Ni_{27}La_8)+xC$ ($x=0$–0.4) alloy electrodes.

Samples	Limiting current density I_L (mA g^{-1})	Activation energy E_a (kJ mol^{-1})
$x=0$	2263.4	38.3
$x=0.15$	2867.4	35.9
$x=0.25$	5692.3	33.7
$x=0.4$	3775.6	34.7

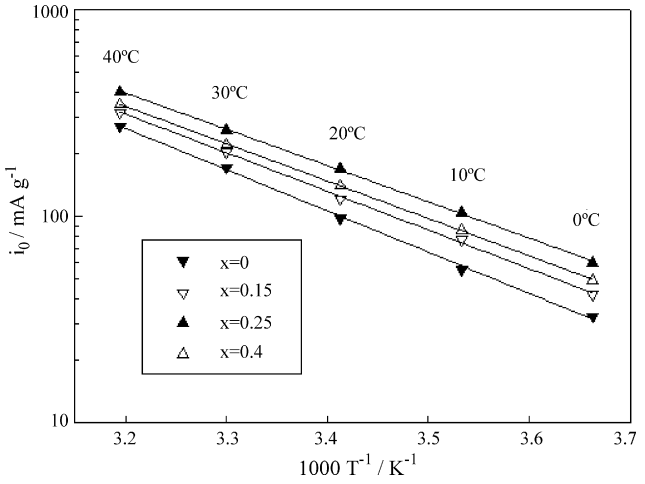

Fig. 6. Arrhenius plots of exchange current density (i_0) for the $(Mg_{65}Ni_{27}La_8)+xC$ (x = 0-0.4) electrodes.

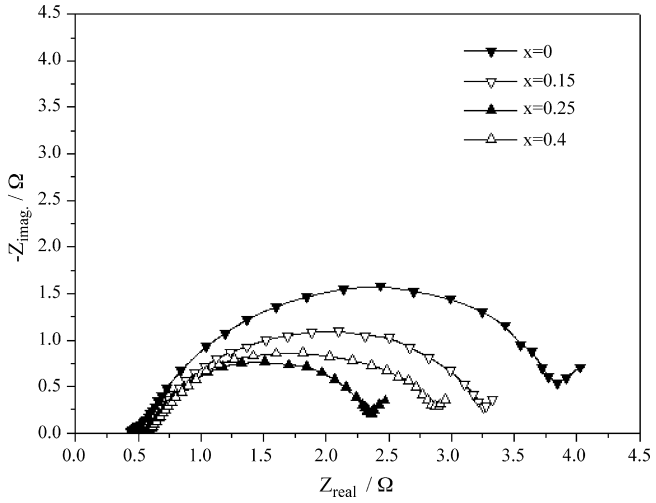

Fig. 7. Electrochemical impedance spectra of the $(Mg_{65}Ni_{27}La_8)+xC$ (x = 0–0.4) electrodes at 50% depth of discharge at 27 °C.

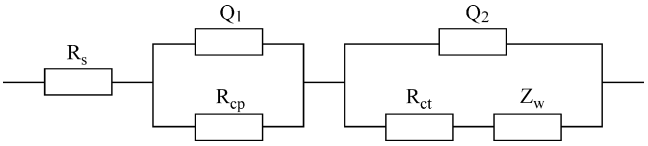

Fig. 8. Equivalent circuit of the electrodes.

Since cracks are formed on the alloy particles during charge/discharge cycles, the electrochemical kinetics of the electrodes should be carefully compared based on the activation energy of charge-transfer reaction, which is independent of change in surface area. The current–potential curves obtained by linear polarization measurement are straight lines for all temperatures. The exchange current densities (i_0) for the electrodes are calculated using the following expression [21]:

$$i_0 = I_d \frac{RT}{F\mu} \quad (1)$$

where R, T, I_d, F, μ are the gas constant, the absolute temperature, the applied current density, the Faraday's constant and the total overpotential, respectively. I_d/μ is the slope of these straight lines. The exchange current density (i_0) is temperature-dependent. It follows the Arrhenius equation:

$$i_0(T) = A \ \exp\left(\frac{-E_a}{RT}\right) \quad (2)$$

where A is a constant, E_a is the apparent activation energy for charge-transfer reaction. Fig. 6 presents Arrhenius plots of the i_0 values for the $(Mg_{65}Ni_{27}La_8)+xC$ (x = 0–0.4) electrodes. The logarithmic i_0 values decrease linearly with an increase in the reciprocal of temperature, and the activation energy for the charge-transfer reaction evaluated from the slope of the plot are listed in Table 2. It decreases first from 38.3 kJ mol^{-1} (x = 0) to 33.7 kJ mol^{-1} (x = 0.25) and then increases to 34.7 kJ mol^{-1} (x = 0.4), indicating the kinetics of electrochemical hydrogen reaction on the surface of alloy is improved. This can be attributed to the increase of electrocatalytic activation by the surface modification.

Fig. 7 shows electrochemical impedance spectra of the $(Mg_{65}Ni_{27}La_8)+xC$ (x = 0–0.4) electrodes. Each spectrum consists of two semicircles in the high-frequency region followed by a straight line in the low-frequency region. According to literature [22], the small arc in the high-frequency region and the large arc in the low-frequency region were assigned to the contact resistance (R_{cp}) between the current collector (Ni foam) and the alloy particles, and to the charge-transfer reaction resistance (R_{ct}) on the alloy surface, respectively. Using the equivalent circuit presented in literature [23], as shown in Fig. 8, we can calculate the values of four different electrodes. The R_s, Z_w and $Q_{1(2)}$ in Fig. 8 represent the solution resistance, the Warburg impedance, and the imperfect capacitor, respectively. The results are listed in Table 3. Both of the R_{cp} and R_{ct} decrease first and then increase with increasing graphite content. In specific, the R_{cp} reduces from 925 mΩ to about 150 mΩ after the surface modification, confirming the result based on morphology analysis. The $(Mg_{65}Ni_{27}La_8)+0.25$ C electrode shows the lowest contact resistance and charge-transfer reaction resistance, suggesting the best electrochemical kinetics.

According to the above results, the influence of graphite modification on the electrochemical characteristics of amorphous $Mg_{65}Ni_{27}La_8$ electrodes could be illuminated as follows. The surface modification by graphite reduces contact resistance between the current collector and the alloy particles, obstructs the formation of $Mg(OH)_2$ on the surface of alloy and increases electrocatalytic activation of the electrodes. Thus, the electrochemical properties of amorphous $Mg_{65}Ni_{27}La_8$ electrodes are improved.

Among them, the increase of electrocatalytic activation seems to be an important factor to improve the electrode properties. Iwakura et al. [24] reported that graphite reacted with amorphous MgNi alloy and probably donated electron density to the alloy surface during high-energy ball milling. The electrons trapped on the alloy surface modified the chemical states of Mg and a graphite–Mg interaction formed on the alloy surface. We think it can increase active sites for hydrogen absorption and desorption and partially prevent the formation of $Mg(OH)_2$ on the alloy surface.

In the electrochemical process, if the alloy surface is covered with $Mg(OH)_2$, it will be difficult for hydrogen atoms to go thought the $Mg(OH)_2$ layer and to react with OH^- and H_2O in the electrolyte. If the alloy surface is covered with graphite, the condition will be different. The diffusion of hydrogen atoms might

Table 3
Contact resistance R_{cp} and charge-transfer resistance R_{ct} of the $(Mg_{65}Ni_{27}La_8)+xC$ (x = 0–0.4) alloy electrodes at 27 °C.

Samples	Contact resistance, R_{cp} (mΩ)	Charge-transfer reaction resistance, R_{ct} (Ω)
x = 0.15	925	3.095
x = 0	156	2.853
x = 0.25	115	1.728
x = 0.4	151	2.457

happen both in the graphite layers and on the graphite surface. The hydrogen-storage capability of graphite is rather low [25], due to its small interlayer distances. Watanabe et al. [26] also mentioned that hydrogen–graphite intercalation compounds (H–GICs) did not form during electrochemical process. Thus, it is also difficult to diffuse hydrogen atoms in the graphite layers. However, Bonfanti et al. [27] reported that hydrogen atoms physisorbed on graphite are highly mobile on the surface even at very low temperature. The diffusion coefficient on the graphite surface is orders of magnitude larger than that on the metal surfaces or in the metals. Therefore, the diffusion of hydrogen atoms on graphite surface is proposed fast than that on or in $Mg(OH)_2$ layer. The appearance of graphite on the alloy surface instead of $Mg(OH)_2$ and the increasing active sites for hydrogen absorption and desorption are expected to be the reason for the decrease of activation energy of charge-transfer reaction or the increase of electrocatalytic activation of the alloy.

When x reaches 0.4, the performance of the $(Mg_{65}Ni_{27}La_8) + 0.4$ C electrode is worse than the $(Mg_{65}Ni_{27}La_8) + 0.25$ C electrode in almost every aspect. This is considered to be caused by two reasons. Firstly, the gaps between $Mg_{65}Ni_{27}La_8$ powder and Ni powder are limited. When the graphite content beyond a certain value, the graphite interlayer between them will becomes thick, and leads to the increase of contact resistance (refer to Table 3), because the electrical conductivity of graphite is not as good as Ni powder. Secondly, further increase of graphite thickness will make the diffusion of hydrogen atoms more difficult, leading to a decrease of electrode properties.

4. Conclusion

The electrochemical characteristics of amorphous $Mg_{65}Ni_{27}La_8$ electrode are greatly improved by surface modification using graphite. The surface modification could enhance the electrocatalytic activity of the alloy, because of the reduction of the activation energy for the charge-transfer reaction. It also reduces the contact resistance of the electrodes and obstructs the formation of $Mg(OH)_2$ on the alloy surface. Therefore, the discharge capacity, cycle life, limiting current density, activation property and discharge potential characteristics of the electrodes are improved. An optimal content ($x = 0.25$) of graphite has been obtained. The $(Mg_{65}Ni_{27}La_8) + 0.25$ C electrode has the largest discharge capacity of 827 mA h g^{-1} and best electrochemical kinetics among the studied electrodes. Further increase of the graphite content will exacerbate the performance of the electrode.

Acknowledgements

We thank Liqun Wang for helpful advice on SEM observation. One of us (D.C. Wu) thanks Xuepeng Li for her support and assistance. The project was supported by the State Key Development Program for Basic Research of China (Grant No. 2007CB707700).

References

[1] L. Schlapbach, A. Züttel, Nature 414 (2001) 353–358.
[2] C. Rongeat, L. Roué, J. Power Sources 132 (2004) 302–308.
[3] S. Mokbli, M. Abdellaoui, H. Zarrouk, M. Latroche, A.P. Guégan, J. Alloys Compd. 460 (2008) 432–439.
[4] S. Todorova, T. Spassov, J. Alloys Compd. 469 (2009) 193–196.
[5] G.Y. Liang, D.C. Wu, L. Li, L.J. Huang, J. Power Sources 186 (2009) 528–531.
[6] L.J. Huang, G.Y. Liang, Z.B. Sun, J. Alloys Compd. 421 (2006) 279–282.
[7] Q.F. Tian, Y. Zhang, L.X. Sun, F. Xu, Z.C. Tan, H.T. Yuan, T. Zhang, J. Power Sources 158 (2006) 1463–1471.
[8] L.J. Huang, G.Y. Liang, Z.B. Sun, Y.F. Zhou, J. Alloys Compd. 432 (2007) 172–176.
[9] H. Niua, D.O. Northwood, Int. J. Hydrogen Energy 27 (2002) 69–77.
[10] T. Abe, S. Inoue, D. Mu, Y. Hatano, K. Watanabe, J. Alloys Compd. 349 (2003) 279–283.
[11] C. Iwakura, H. Inoue, S.G. Zhang, S. Nohara, J. Alloys Compd. 293–295 (1999) 653–657.
[12] S. Nohara, H. Inoue, Y. Fukumoto, C. Iwakura, J. Alloys Compd. 252 (1997) L16–L18.
[13] C. Iwakura, H. Inoue, S. Nohara, R. Shin-ya, S. Kurosaka, K. Miyanohara, J. Alloys Compd. 330–332 (2002) 636–639.
[14] S. Ruggeri, L. Roué, G. Liang, J. Huot, R. Schulz, J. Alloys Compd. 343 (2002) 170–178.
[15] K. Funaki, S. Orimo, H. Fujii, H. Sumida, J. Alloys Compd. 270 (1998) 160–163.
[16] Z.P. Guo, Z.G. Huang, K. Konstantinov, H.K. Liu, S.X. Dou, Int. J. Hydrogen Energy 31 (2002) 2032–2039.
[17] L.J. Huang, G.Y. Liang, Z.B. Sun, D.C. Wu, J. Power Sources 160 (2006) 684–687.
[18] L. Li, D.C. Wu, G.Y. Liang, Z.B. Sun, Y.L. Guo, J. Alloys Compd. 474 (2009) 378–381.
[19] L. Aymard, C. Lenain, L. Courvoisier, F. Salver-Disma, J.M. Tarascon, J. Electrochem. Soc. 146 (1999) 2015–2023.
[20] W. Liu, Y. Lei, D. Sun, J. Wu, Q. Wang, J. Power Sources 58 (1996) 243–247.
[21] P.H.L. Notten, P. Hokkeling, J. Electrochem. Soc. 138 (1991) 1877–1885.
[22] N. Kuriyama, T. Sakai, H. Miyamura, I. Uehara, H. Ishikawa, T. Iwasaki, J. Alloys Compd. 202 (1993) 183–197.
[23] Q. Liu, L.F. Jiao, H.T. Yuan, Y.J. Wang, Y. Feng, J. Alloys Compd. 427 (2007) 275–280.
[24] C. Iwakura, H. Inoue, S.G. Zhang, S. Nohara, K. Yorimitsu, N. Kuramoto, T. Morikawa, J. Electrochem. Soc. 146 (1999) 1659–1663.
[25] R. Ströbel, J. Garche, P.T. Moseley, L. Jörissen, G. Wolf, J. Power Sources 159 (2006) 781–801.
[26] M. Watanabe, M. Tachikawa, T. Osaka, Electrochim. Acta 42 (1997) 2707–2717.
[27] M. Bonfanti, R. Martinazzo, G.F. Tantardini, A. Ponti, J. Phys. Chem. C 111 (2007) 5825–5829.